Evaluation of Dislocation Density of Coarse and Fine Grains in Bimodal Harmonic Structured Steel Observed by Diffraction Contrast Tomography using Ultrabright Synchrotron···

Nakai, Yoshikazu ; Kikuchi, Shoichi ; Shiozawa, Daiki ; Hase, Takumi ; Nakazawa, Issei ; Fujita, Keisuke ; Kawabata, Mie O. ; Ameyama, Kei

Evaluation of Dislocation Density of Coarse and Fine Grains in Bimodal Harmonic Structured Steel Observed by Diffraction Contrast Tomography Using Ultrabright Synchrotron Radiation

Yoshikazu Nakai[1]*, Shoichi Kikuchi[2], Daiki Shiozawa[1], Takumi Hase[1], Issei Nakazawa[1], Keisuke Fujita[3], Mie O. Kawabata[4], and Kei Ameyama[4]

[1] Department of Mechanical Engineering, Kobe University, 1-1, Rokkodai, Nada, Kobe 657-8501, Japan
E-mail: nakai@mech.kobe-u.ac.jp
[2] Department of Mechanical Engineering, Shizuoka University, 3-5-1, Johoku, Naka, Hamamatsu 432-8561, Japan
[3] Graduate School of Science and Technology, Shizuoka University, 3-5-1, Johoku, Naka, Hamamatsu 432-8561, Japan
[4] Department of Mechanical Engineering, Ritsumeikan University, 1-1-1, Noji Higashi, Kusatsu 525-8577, Japan

Austenitic stainless steels with a bimodal harmonic structure, in which the fine grain structure (Shell) exists around the coarse grain structure (Core), are prepared by powder metallurgy to improve both strength and ductility. In this study, X-ray diffraction contrast tomography, a three-dimensional grain mapping technique for polycrystalline materials using ultrabright synchrotron radiation X-rays, is used to reconstruct the grain shape and location and to evaluate the average excess dislocation density of the Core and Shell structures. This technique allows us to evaluate the excess dislocation density not only on the surface, but also inside the sample where damage occurs in tensile tests. The results show that the excess dislocation density of the Shell structure is higher than that of the Core structure. The excess dislocation density of homogeneous austenitic stainless steels with grain sizes similar to the Core structure of the harmonic structured stainless steel is higher than that at comparable stresses, indicating that the deformation of the bimodal harmonic structured alloy is localized in the fine grain structure. This is consistent with the results obtained from electron backscatter diffraction analysis, in which the surface grains are evaluated.

1. Introduction

Since metallic materials are often used for mechanical and structural components subject to high stress, various methods have been developed to obtain high-strength metallic materials. Among them, grain refinement is effective in increasing the strength of metallic materials, but it usually causes plastic instability and necking, resulting in the loss of ductility. To resolve this tradeoff between strength and ductility, Ameyama et al. combined grain refinement and powder metallurgy to create a "harmonic structured material" in which high-strength grains are arranged in a network around coarse grains with high ductility [1-8]. The three-dimensional periodic structure of this harmonic structured material can suppress necking and achieve high strength and ductility [3]. Nakai et al. [9] observed, by phase contrast tomography using ultrabright synchrotron radiation X-rays, macroscopic deformation and geometrical defect during the tensile test of the harmonic structured materials.

Several recent studies have focused on investigating plastic deformation in harmonic structured materials to understand the stress partitioning and deformation of fine and coarse grains [10-14]. These studies have revealed that from the early stages of plastic deformation, stresses and strains are divided into grains in Core and Shell structures. However, direct quantitative measurements of stresses have not been conducted. In situ X-ray diffraction (XRD) analysis can capture the average behavior within coarse and fine grains, making it possible to directly determine stress partitioning.

In multiphase materials, diffraction peaks from different phases are often easily distinguished because they appear at different diffraction angles. For single-phase materials with heterogeneous grain sizes, however, the separation is more complex because diffraction peaks from coarse and fine grains appear at the same diffraction angles. Matěj et al. [15] found large recrystallization-free defect-free grains and ultrafine grains with high dislocation-density in pure polycrystalline copper samples treated with an equal channel anguar pressing (ECAP). They presented a peak-broadening-based method for separating diffraction peaks and stated that it is a suitable method for determining the relative proportions of microstructural components as well as other parameters (*e.g.*, dislocation density). However, Sjögren-Levin et al. [16,17] reported that no significant differences in size broadening can be expected between the fractions of harmonic structured materials with average grain sizes in Shell and Core structures significantly larger than 1 μm, making the broadening-based method inapplicable. Furthermore, as reported by Lin et al. [18], it is not possible to distinguish different fractions from a particular textural component. Sjögren-Levin et al. [16,17] developed a procedure tailored to the collection of XRD data for materials with heterogeneous grain sizes, along with

an algorithm to separate the average diffraction signal from grains of different sizes, determined the strain for each grain size and evaluated the accuracy of the algorithm.

Recently, dislocation density has usually been evaluated by electron backscattering diffraction (EBSD) analysis, which yields the dislocation density at the sample surface, where plane stress conditions prevail, whereas damage in tensile test always occurs inside the sample, where plane strain conditions prevail.

Ludwig et al. [19] proposed diffraction contrast tomography (DCT), which uses ultrabright synchrotron radiation X-rays to reconstruct the shape and position of each particle in a polycrystalline material. Nakai et al. developed a method of evaluating misorientation, defined as the orientation spread of diffraction spots and corresponding to the number of excess dislocations in the diffraction plane, using DCT [20]. DCT can be used to observe the misorientation of each grain not only on the sample surface but also inside the sample, as reported by Shiozawa et al. [21,22] and Nakai et al. [20,23,24]. It is a nondestructive observation technique that enables the continuous observation of the local plastic deformation of grains not only on the sample surface but also inside the sample.

In this study, we measured the excess dislocation density of grains in the Shell and Core structures by DCT to elucidate the unique mechanical properties of harmonic structured materials.

2. Experimental Procedures

2.1. DCT imaging

Figure 1 shows an overview of the DCT imaging geometry. When the sample is irradiated with X-rays, diffraction occurs at the grains that satisfy the Bragg condition. Diffraction spots appear in the direction of the diffraction angle, and dark extinction spots appear behind the sample.
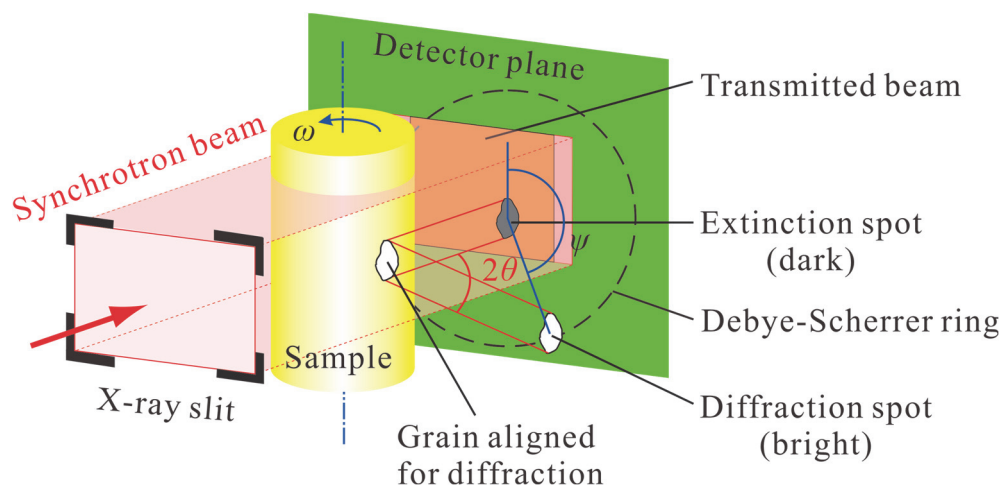

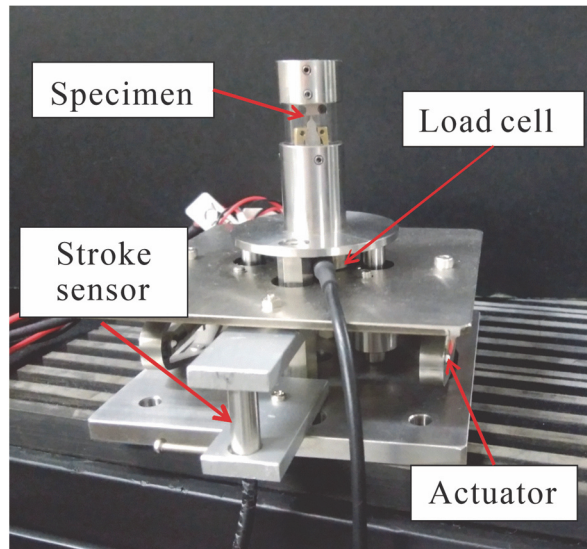Figure 1 Overview of DCT imaging geometry.

Figure 2 Geometrical relation between misorientation, spread of rotation angle, diffraction angle, and Debye-Scherrer ring angle for grains satisfying Bragg condition.

The total misorientation n be calculated by measuring the spread of the rotation angle $\Delta\omega_{\text{diff}}$, diffraction angle θ, and Debye-Scherrer ring angle ψ of the grain satisfying the Bragg condition for each diffraction spot, as shown in **Figure 2** [22,24].

$$\beta = \Delta\omega_{\text{diff}} \sin\phi \qquad (1)$$

Here, ϕ is the angle between the normal of the diffraction plane and the rotation axes, and is given by

$$\phi = \cos^{-1}\left(\cos\theta\cos\psi\right). \qquad (2)$$

Excess dislocation density ρ can be estimated as [25]

$$\rho = \frac{\beta}{bd}, \qquad (3)$$

where b is Burger's vector and d is grain size.

DCT imaging was performed using the BL46XU beamline of the synchrotron radiation facility of Super Photon ring 8 GeV (SPring-8), which uses an undulator beam and provides an X-ray beam with ultrabright high spatial coherence, enabling microtomography with high spatial resolution in the μm range. The polychromatic synchrotron radiation beam was monochromatized to an energy of 37 keV using a Si{111} double-crystal monochromator. 2-D projected images were recorded with a high-resolution detector system with a transparent luminescent screen, light optics, and a charge-coupled device (CCD) camera. The distance between the sample and the detector must be sufficiently short to detect as many diffraction spots as possible, so it was set to 10 mm. An effective pixel size of 2.7 μm was used for the experimental projection images. To detect diffraction spots, the beam size at the sample position

Figure 3 Stepping motor-driven tensile testing machine.

was limited to 1.0 mm × 1.0 mm by using an X-ray slit. The projection images were acquired at 0.05° intervals over 360°. The acquisition time of each DCT data was 75 min. The imaging apparatus of DCT is given by Nakai et al. elsewhere [24].

The stepping-motor-driven tensile test machine shown in **Figure 3** was used for inline test [25]. The machine used was small enough to be placed on a rotating stage for tomographic imaging. The displacement rate of the tensile test was 1.0 μm/min.

2.2. Materials and specimen

Austenitic stainless steels JIS-SUS304L and SUS316L powder were used to prepare the samples. First, JIS-SUJ2 balls and stainless steel powder were placed in the carbide container of a planetary ball mill, and the surface particles of the initial powder were refined by mechanical milling. Milling was performed at room temperature in an argon environment at a pot speed of 200 rpm with a processing time of 50 or 20 h, as shown in **Table 1**, where the diameter of the powder used for Compact B is larger than that for Compact A. The mechanically milled powder was then pressed by spark plasma sintering (SPS) to produce a harmonic

Table 1. Conditions for preparation of samples.

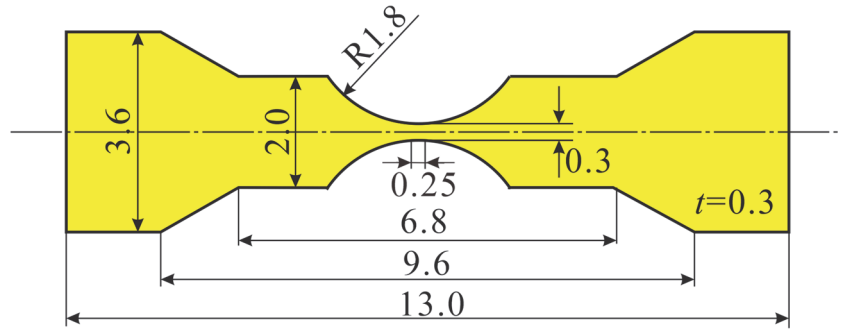| Compact	Powder Diameter [μm]	Spark plasma sintering				
		Mechanical milling [h]	Temperature [°C]	Pressure [MPa]	Duration [h]	Sintering mold size [mm]
Compact A	SUS304L 120	50	950	50	1	25
Compact B	SUS316L 170	20	1000	50	1	30

Figure 4 Shapes and dimensions of the tensile test specimens (Dimensions in mm).

structured material (Harmonic series). Details of the SPS conditions are shown in **Table 1**. SPS was followed by furnace cooling. For comparison, a homogeneous coarse-grained material was prepared by sintering the initial powder without mechanical milling (Homogeneous series). Hereafter, the sintered material prepared from SUS304L is referred to as Compact A and that prepared from SUS316L powder is referred to as Compact B. Only the Harmonic series of Compact A (Harmonic-A) was measured for relative density, which was 99.6%, indicating that there was almost no porosity.

Harmonic-A is a standard harmonic structured material; however, DCT cannot be conducted for grains smaller than 10 μm, so only grains in the Core structure could be measured. Then, a special harmonic structured material of Compact B (Harmonic-B), in which the grains in the Shell and Core structures were sufficiently large, was fabricated for the DCT of grains in both structures.

The shapes and dimensions of the tensile test specimens cut by electrical discharge machining (EDM) from the sintered material are shown in **Figure 4**, where the smallest cross section of each specimen is 0.3 mm × 0.3 mm square and the length of the parallel section is 0.25 mm.

3. Experimental Results

3.1. Microstructural analysis

Prior to DCT imaging, the microstructure of the Harmonic series was analyzed using EBSD. **Figures 5** and 6 are the inverse pole figure (IPF) and grain size maps of Harmonic series, respectively. Grain boundaries were defined as boundaries with an orientation difference of 15° or greater and are indicated by black lines, where twins were considered as individual grains in the evaluation of grain size and dislocation density. It can be seen that fine grains are formed around the coarse grains. The average grain sizes of the materials measured by EBSD analysis are shown in **Table 2**, where grains smaller than 10 μm for Compact A and 40 μm for Compact B were defined as Shell grains. The fraction of number of grains in Shell in Compact A and Compact B are 42 % and 65 %, respectively.
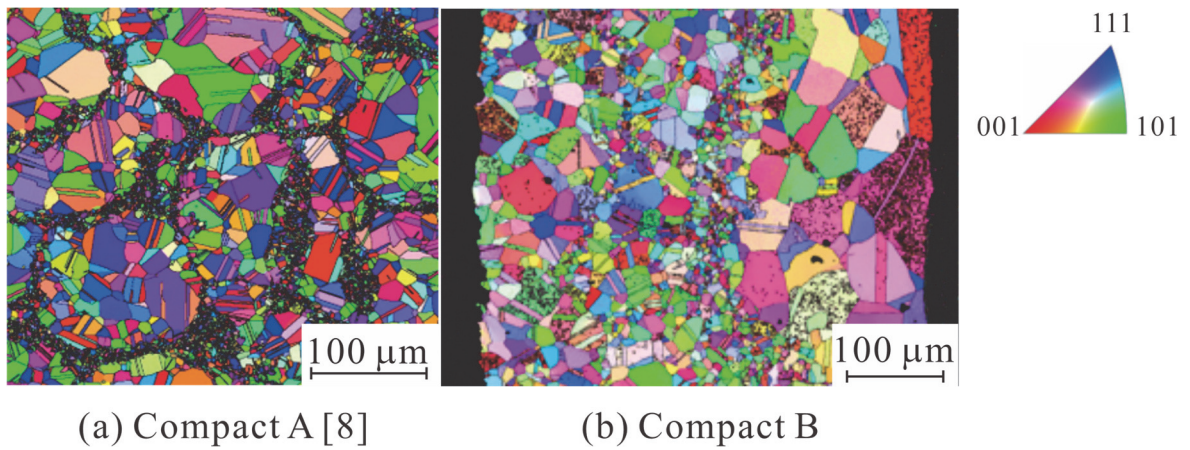
(a) Compact A [8] (b) Compact B

Figure 5 Inverse pole figure (IPF) maps obtained from the EBSD analysis for Harmonic series.

(a) Compact A (Harmonic)

Average grain size

Shell: 1.8 [μm] Fraction 42 [%]
Core: 15.6 [μm] 58 [%]

(b) Compact B (Harmonic)
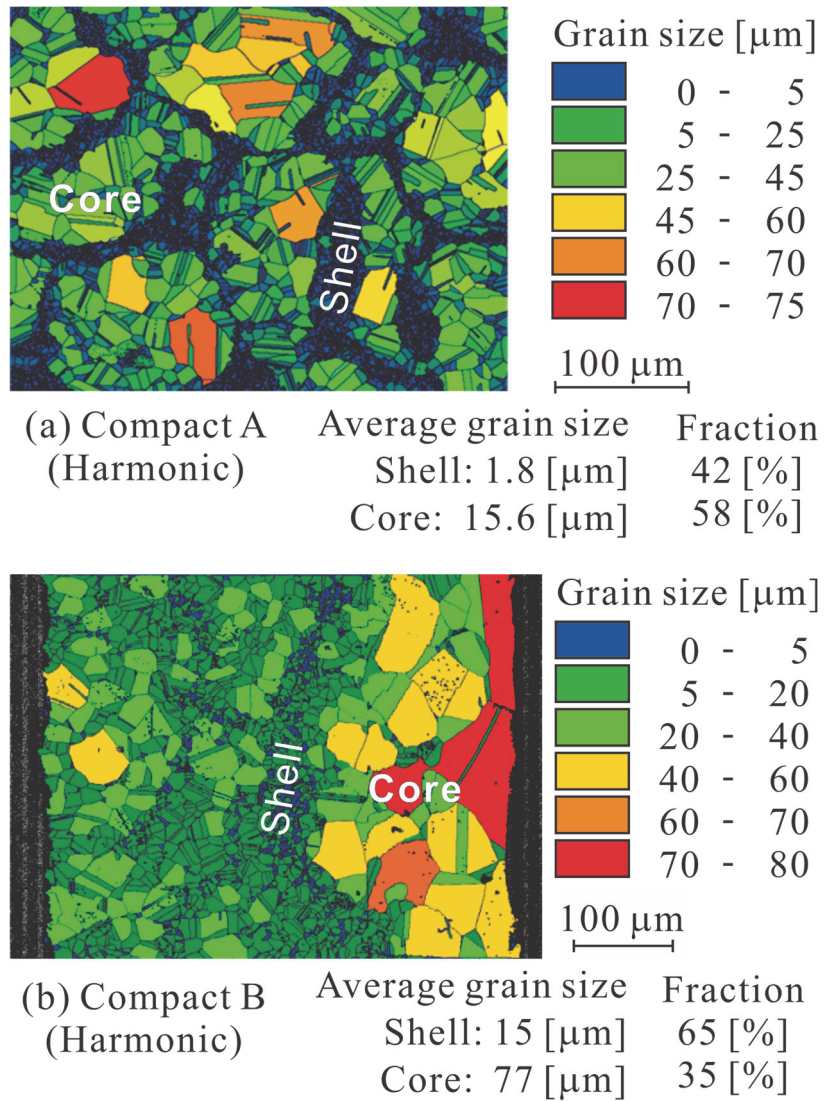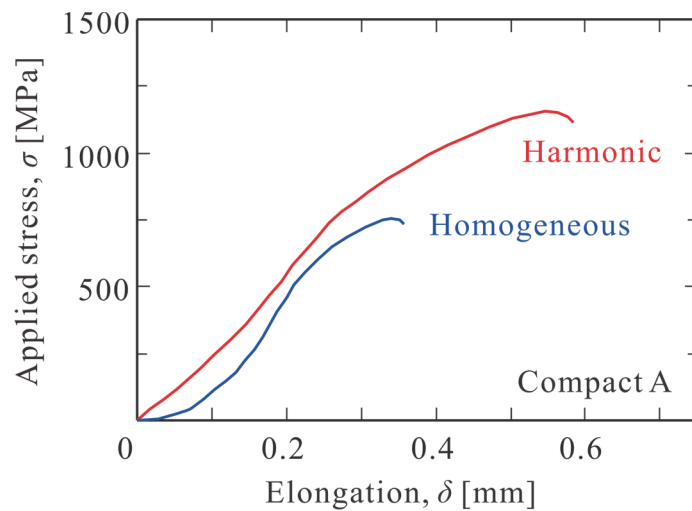
Average grain size

Shell: 15 [μm] Fraction 65 [%]
Core: 77 [μm] 35 [%]

Figure 6 Grain size maps obtained from the EBSD analysis for Harmonic series.

Table 2. Average grain sizes.

	Compact A			Compact B		
	Homogeneous series	Harmonic series		Homogeneous series	Harmonic series	
		Core	Shell		Core	Shell
Grain size [μm]	33	16.8	2.1	33	77.6	15.4

3.2. Stress–elongation relationships

Because of the small size of the specimen, it was not possible to measure the elongation of the parallel part of the specimen. Therefore, the distance between grips was measured by a stroke sensor (see **Figure 3**), and anomalous curve was obtained for a Homogeneous series as shown in **Figure 7**(a). This could be due to imperfect gripping. As shown in **Figure 7**, for both

(a) Compact A

(a) Compact B

Figure 7 Stress-elongation relationships, where elongation is the displacement between grips.
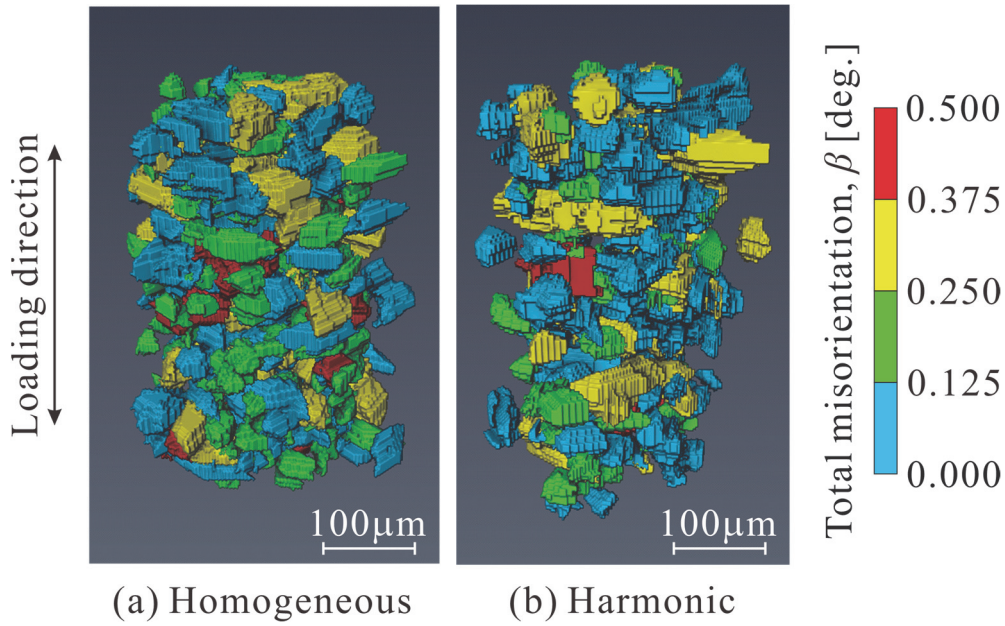
Figure 8 Examples of DCT reconstructions of grains in Homogeneous series and Harmonic series before tensile test (Compact A).

compacts, the strength of the Harmonic series is higher than that of the Homogeneous series. The elongation at fracture is also significantly greater for the Harmonic series than Homogeneous series.

3.3. Reconstruction of grains

Figure 8 shows examples of DCT reconstructions of grains in Homogeneous series and Harmonic series of Compact A before the tensile test. The color indicates the degree of misorientation of each grain. In the Homogeneous series, most of the grains are successfully reconstructed, while in the Harmonic series, only the grains of the Core structure are reconstructed.

3.4. Misorientation and excess dislocation density

The change in total misorientation for each diffraction plane during the tensile test is shown in **Figure 9**, where the values are averaged for all grains. For either diffraction plane, the average total misorientation β_{ave} is almost unchanged in the elastic region, but increases significantly in the plastic deformation region. For commercially pure iron, the change in average total misorientation is reported to be the greatest in the slip plane [21], while the change is similar for all diffraction planes in the present material.

Figure 10 shows the change in the average excess dislocation density of Harmonic series and Homogeneous series in the tensile test for Compact A, where the values for Harmonic series are those for grains in the Core structure; averaging was conducted for all diffraction planes including all grains. The change in excess dislocation density is smaller for the Core structure
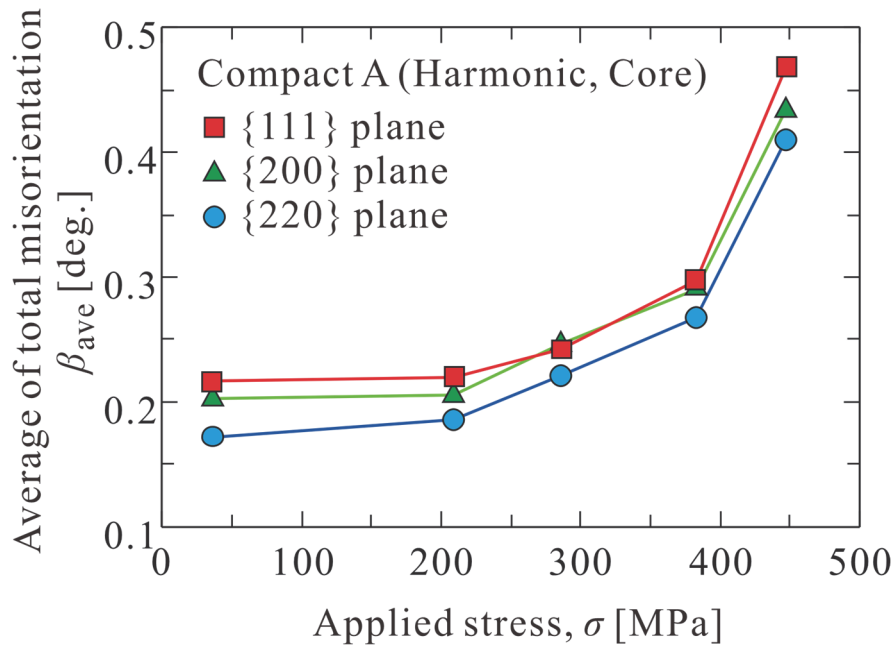
Figure 9 Change in total misorientation for each diffraction plane during the tensile test (Compact A, Hamonic series).
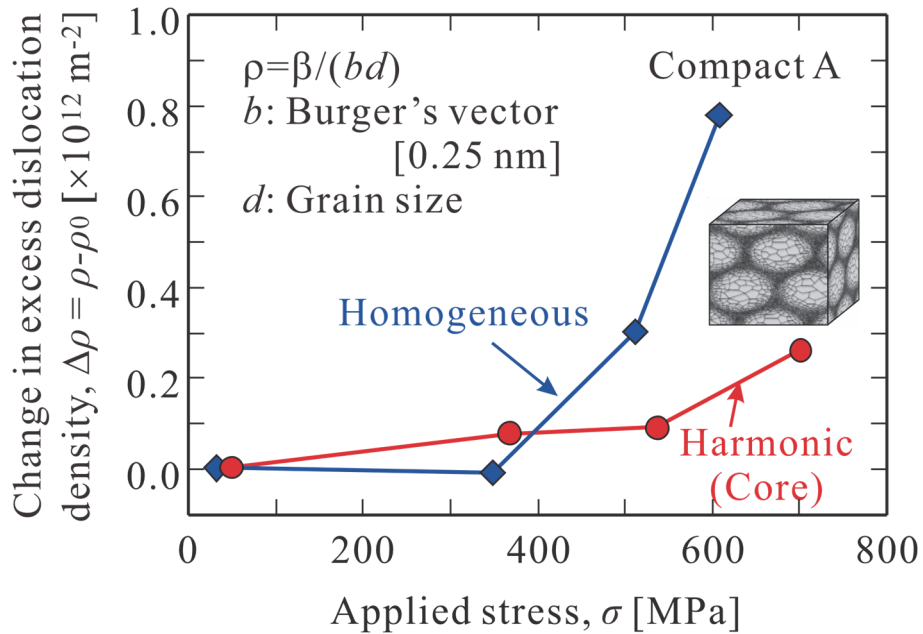

Figure 10 Change in excess dislocation density in the Core structure of Harmonic series and Homogeneous series in tensile test for Compact A, where ρ_0 is the initial dislocation density.

in Harmonic series than for that in Homogeneous series at a comparable stress. This result suggests that the Core structure is less deformable than the Shell structure in the Harmonic series and that the deformation is localized in the Shell structure.
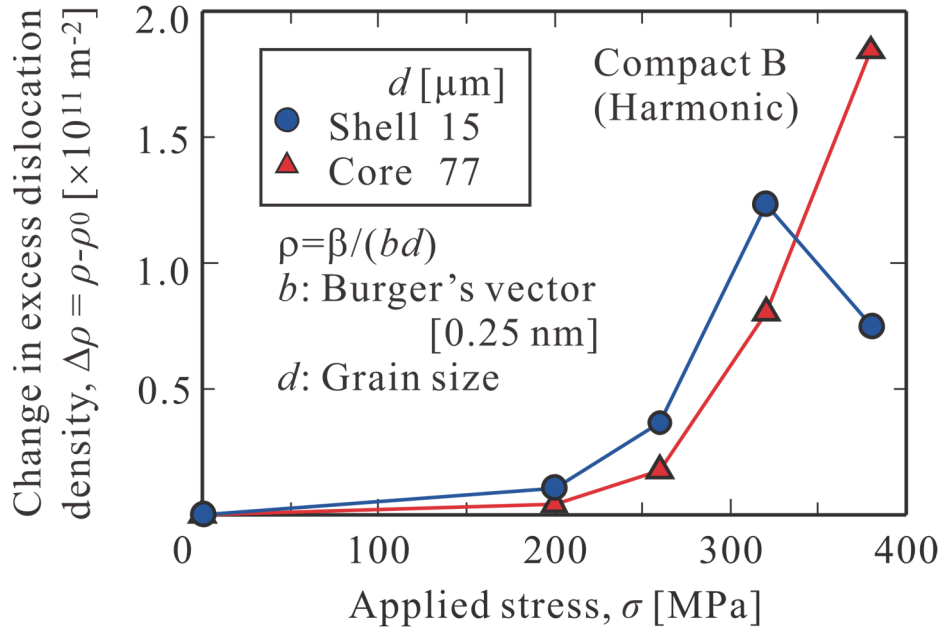
Figure 11 Change in excess dislocation density of grains in the Core structure and those in the Shell structure of Harmonic series in tensile test for Compact B, where ρ_0 is the initial dislocation density.

The change in the average excess dislocation density of grains in the Core structure and those in the Shell structure of Harmonic series obtained from Compact B is shown in **Figure 11**. The excess dislocation density increases monotonically with stress for the grains in the Core structure, but decreases at the end of the test for the grains in the Shell structure. This is because the diffraction spots become too dark to observe when the excess dislocation density is very high, and the diffraction spots were averaged only for the grains with low excess dislocation density. Except for such data, the change in excess dislocation density is smaller for grains in the Core structure than for grains in the Shell structure at the same applied stress. This result also indicates that the deformation of harmonic structured materials is localized in the Shell structure.

On the basis of the results of EBSD analysis, Ameyama et al. [26] reported that for harmonic structured materials, microdeformation mainly occurs in the network of fine grains and suppresses the deformation of the Core structure. In the present study, we could directly measure the dislocation density in the Shell structure, and could clarify the deformation mechanism unique to harmonic structural materials.
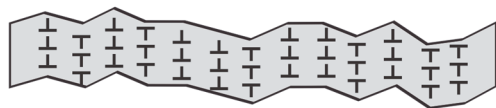
4. Discussion

The radius of the Debye-Scherrer rings obtained by the XRD analysis of polycrystalline materials is inversely proportional to the distance between the diffraction planes. From this

difference in radius, elastic strain or stress can be measured. This measurement is usually performed with a one-dimensional detector. In this case, it is necessary to obtain a continuous Debye-Scherrer ring because of the presence of many grains in the X-ray-irradiated area in order to obtain consistent results independent of the measurement position in the Debye-Scherrer ring. Then, the measured elastic strain would be the average of the strain of each grain, and the elastic strain of individual grains would not be measurable.
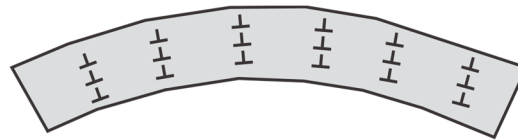
On the other hand, the atomic spacing within a single grain changes owing to the presence of dislocations, resulting in the radial spread of the Debye-Sherrer ring. This spread can be used to determine the average dislocation density. It has been reported that the dislocation density measured by this method agrees well with transmission electron microscopy (TEM) results [27]. With an X-ray microbeam and a two-dimensional detector, the number of grains in the X-ray-irradiated area is found to be small and individual diffraction spots are separated, making it possible to measure micro–lattice strain from the radial spread of the Debye-Sherrer ring and excess dislocation density from the circumferential spread of the ring [28,29]. The excess dislocation density is the difference between the positive and negative dislocation densities, and is different from the total dislocation density measured by the radial spread of Debye-Sherrer ring method and TEM.

Since DCT utilizes diffraction spots from transmitted X-rays, the number of grains in the X-ray-irradiated area is small because a small sample is employed, and separated diffraction spots similar to those produced by X-ray microbeams are obtained. With an X-ray microbeam, only diffraction from grains on the sample surface is observed, so the distance between the diffracted grains and the detector can be accurately measured. On the other hand, diffraction from internal grains is also observed for DCT, so the position of the grains must be accurately evaluated. However, at present, the positional accuracy of the grains in DCT is insufficient for measuring lattice strain.

In this study, we classified the grains in the Shell and Core structures in accordance with the size of diffraction spots. The average excess dislocation density of grains belonging to each structure was evaluated from the average misorientation of each structure. The results show that the average dislocation density of grains in the Shell structure is higher than that of grains in the Core structure, indicating that it is important to understand the deformation behavior within the Shell structure. However, even within the Shell structure, the deformation behavior should be different between grains adjacent to and away from the Core/Shell boundary. At present, the analysis of the dislocation density of individual grains within the Shell and Core structures has not been completed, but this will be accomplished in future studies.

(a) Gaussian distribution
(Typically in fatigue)

(b) Uniform distribution
(Typically in uniaxial tension)

Figure 12 Deformation mode of grain.

The relationship between misorientation and dislocation density in Equation (3) depends on the deformation mode of the grains, as shown in **Figure 12** [25,28], but it is not expected to affect the comparison between the excess dislocation densities of the Core and Shell structures because the deformation mode is considered to be the same for single-phase materials with different grain sizes.

In the future, we would like to develop a method for the precise evaluation of the location of grains so that we can evaluate not only the three-dimensional shape of each grain but also both excess dislocation density and lattice strain, in order to elucidate the deformation mechanism specific to harmonic structured materials in greater detail.

4. Conclusions

In the present study, tensile tests were performed on austenitic stainless steels with harmonic structures. At the same time, DCT using ultrabright synchrotron radiation X-rays was successfully performed to measure the excess dislocation density of fine grains in the Shell structure and that of coarse grains in the Core structure separately. The following results were obtained:

1. The trend of change in total misorientation owing to plastic deformation was similar regardless of the diffraction plane.

2. The excess dislocation density of the grains in the Core structure of the harmonic structured material was lower than that of the grains in the homogeneous material without a harmonic structure.

3. The excess dislocation density of grains in the Core structure of the harmonic structured material was lower than that in the Shell structure.

4. The fact that the excess dislocation density in the Shell structure consisting of fine grains is lower than that in the Core structure consisting of coarse grains indicates that the deformation of the bimodal harmonic structured material is localized in the Shell structure.

References

[1]   A. Ueno, H. Fujiwara, M. Rifai, Z. Zhang, K. Ameyama, J. Soc. Mater. Sci. Japan, **2021**, 61, 686.

[2]   Z. Zhang, SK. Vajpai, D. Orlov, K. Ameyama, Mater. Sci. Eng. A, **2014**, 598, 106.

[3]   Z. Zhang, D. Orlov, S.K. Vajpai, B. Tong, K. Ameyama, Adv. Eng. Mat., **2015**, 17, 791.

[4]   Z. Zhang, H. Ma, R. Zheng, Q. Hu, M. Nakatani, M. Ota, G. Chen, X. Chen, C. Ma, K. Ameyama, Mater. Sci. Eng. A, **2017**, 707, 287.

[5]   P.K. Rai, S. Shekhar, M. Nakatani, M. Ota, S.K. Vajpai, K. Ameyama, K. Mondal, Metallur. Mater. Trans. A, **2016**, 47, 6259.

[6]   P.K. Rai, S. Shekhar, M. Nakatani, M. Ota, S.K. Vajpai, K. Ameyama, K. Mondal, J. Mater. Eng. Perform., **2017**, 26, 2608.

[7]   H.K. Park, K. Ameyama, J. Yoo, H. Hwang, Kim, Mater. Res. Lett., **2018**, 6, 261.

[8]   Kikuchi, Y. Nukui, Y. Nakatsuka, Y. Nakai, M. Nakatani, M.O. Kawabata, K. Ameyama,Int. J. Fatigue, **2019**, 127, 222.

[9]   Y. Nakai, S. Kikuchi, D. Shiozawa, I. Nakazawa, K. Fujita, M.O. Kawabata, K. Ameyama. Procedia Struct. Integ., **2023**, 43, 221.

[10]   A. Shokry, A. Ahadi, P. Ståhle, D. Orlov, Sci. Rep., **2021**, 11 17445.

[11]   D. Orlov, H. Fujiwara, K. Ameyama, Mater. Trans., **2013**, 54 1549.

[12]   H.K. Park, K. Ameyama, J. Yoo, H. Hwang, H.S. Kim, Mater. Res. Lett., **2018**, 6 261.

[13]   D. Orlov, J. Zhou, S. Hall, M.O. Kawabata, K. Ameyama, IOP Conf. Ser. Mater. Sci. Eng., **2019**, 580 012019.

[14]   D. Orlov, R. Kulagin, Y. Beygelzimer, Mater. Lett., **2020**, 275 128126.

[15]   Z. Matěj, A. Kadlecová, M. Janeček, L. Matějová, M. Dopita, R. Kužel, Powder Diffr, **2014**, 29 S35.

[16]   E. Sjögren-Levin, W. Pantleon, A. Ahadi, Z. Hegedüs, U. Lienert, N. Tsuji, K. Ameyama, D. Orlov, Mater. Sci. Eng., **2022**, 1249, 012040.

[17]   E. Sjögren-Levin, W. Pantleon, A. Ahadi, Z. Hegedüs, U. Lienert, N. Tsuji, K. Ameyama, D. Orlov, Scripta Materialia 226 (2023) 115186.

[18] F.X. Lin, Y.B. Zhang, W. Pantleon, D. Juul Jensen, Philos. Mag., **2015**, 95, 2427.

[19] S. Ludwig, W. Schmidt, E.M. Lauridsen, H.F. Poulsen, J. App. Cryst., **2008**, 41, 302.

[20] Y. Nakai, D. Shiozawa, R. Nakao, N. Asakawa, S. Kikuchi, Mater. Sci. Forum, **2016**, 879, 1355.

[21] D. Shiozawa, Y. Nakai, R. Miura, S. Matsuda, Adv. Mater. Res., **2014**, 891-892, 600.

[22] D. Shiozawa, Y. Nakai, R. Miura, N. Masada, S. Matsuda, R. Nakao, Int. J. Fatigue, **2016**, 82, 247.

[23] Y. Nakai, D. Shiozawa, J. Soc. Mater. Sci. Japan, **2017**, 66, 621.

[24] Y. Nakai, D. Shiozawa, N. Asakawa, K. Nonaka, S. Kikuchi, Proc. Struct. Integ., **2017**, 3, 402.

[25] P. Gay, P.B. Hirsch, A. Kelly, ACTA Metallur., **1953**, 1, 315.

[26] K. Ameyama, F. Cazes, H. Couque, G. Dirras, S. Kikuchi, J. Li, F. Mompiou, K. Mondal, D. Orlov, B. Sharma, D. Tingaud, S.K. Vajpai, Mater. Res. Lett., **2022**, 107, 440.

[27] K. Prasad, M. Obana, A. Ito, S. Torizuka, Mater. Charact., **2021**, 179, 111379.

[28] S. Taira, K. Hayashi, Bulletin of JSME, **1967**, 9, 627.

[29] Y. Nakai, K. Tanaka, T. Nakanishi, Eng. Fract. Mech., **1981**, 15, 291.

List of Tables and Figures

Table 1   Conditions for preparation of samples.

Table 2   Average grain sizes.

Figure 1   Overview of DCT imaging geometry.

Figure 2   Geometrical relation between misorientation, spread of rotation angle, diffraction angle, and Debye-Scherrer ring angle for grains satisfying Bragg condition.

Figure 3   Stepping motor-driven tensile testing machine.

Figure 4   Shapes and dimensions of the tensile test specimens (in mm).

Figure 5   Inverse pole figure (IPF) maps obtained from the EBSD analysis for Harmonic series.

Figure 6   Grain size maps obtained from the EBSD analysis for Harmonic series.

Figure 7   Stress-elongation relationships, where elongation is the displacement between grips.

Figure 8   Examples of DCT reconstructions of grains in Homogeneous series and Harmonic series before tensile test (Compact A).

Figure 9   Change in total misorientation for each diffraction plane during the tensile test (Harmonic-A).

Figure 10   10 Change in excess dislocation density in the Core structure of Harmonic series and Homogeneous series in tensile test for Compact A, where ρ_0 is the initial dislocation density.

Figure 11   Change in excess dislocation density of grains in the Core structure and those in the Shell structure of Harmonic series in tensile test for Compact B, where ρ_0 is the initial dislocation density.

Figure 12   Deformation mode of grain.